Estimation of expected challenge levels for support of chemical biological and radiological defensive measures: Canadian methodology

Eugene Yee

Defence R&D Canada, Suffield Research Centre, P.O. Box 4000 Stn Main, Medicine Hat, Alberta, Canada T1A 8K6

1. Introduction

Toxic materials can be released into the atmosphere as a result of natural hazards (e.g., volcanic eruptions, wildfires), of technological hazards involving accidental releases from power facilities, industrial sites and vehicles transporting hazardous materials (e.g., tanker collisions, train derailments), and of the intentional use of chemical, biological, radiological and nuclear (CBRN) agents by individual terrorist organizations and affiliates or by rogue state actors. In any toxic agent release, solid, liquid and/or gaseous contaminants may be released from either fixed or mobile sources. When a toxic agent is released into the atmosphere, a number of key questions need to be addressed such as: “What is the nature of the hazard?”, “What is the extent of the toxic corridor for the hazard?”, “What is the risk to personnel exposed?”, “How do we respond to the hazard?”, etc. (see Figure 1). Hazard modeling, which provides the ability to predict and track the effective dispersion of windborne toxic agents, may be used to obtain quantitative answers to some of these key questions. Consequently, hazard modeling for the determination of expected challenge levels has become a critical element that has been used by both civilian and military authorities for planning, response, training, mission rehearsal, and quantitative assessment of risks accruing from these types of releases. In addition, hazard modeling is used to support the development of defensive and protective measures required for defence planning (e.g., concept development and experimentation, test and evaluation, intelligence, operational analysis) and procurement programs (e.g., simulation-based acquisition, rapid prototyping).

Consequence assessment (focused on the response of people, equipment, and structures to the damaging effects of the hazardous material), when used in conjunction with predictions of the atmospheric transport and diffusion of toxic agents, has become increasingly important in recent years. As a result, there has been a considerable effort focused on the accurate prediction of concentration (challenge) levels that result from the release of a toxic material

into the atmosphere. Generally, the prediction of challenge levels requires sophisticated atmospheric transport and diffusion models that can predict the dispersion of the plume as a function of space and time. In particular, the construction of robust models for challenge level estimation in the CBRN domain is difficult because of the lack of phenomenological knowledge of various physical processes that might occur in the dispersion of the toxic agent in the environment and of the uncertainty in various model input parameters. Nevertheless, these models have played an increasingly important role in consequence assessment and in emergency response systems for releases of hazardous materials. They have been used for calculating the transport, diffusion, deposition, secondary evaporation, and resuspension of toxic chemical, biological or radiological materials released (either accidentally or deliberately) into the atmosphere over complex terrain (including over "complex" surfaces such as cities and other built-up environments). Indeed, over the past decade or so, dispersion modeling systems that can make predictions of the highly disturbed urban flow (i.e., turbulent flow in cities) and of the concomitant dispersion of CBRN agents released into this complex flow have become increasingly available.

- Natural disasters
  - Volcanic eruptions
  - Forest fires
- Toxic industrial chemicals
- RDDs (radiological agents)
- Chemical warfare agents
- Biological agents/toxins

What is the nature of the hazard?
What is extent of toxic corridor for hazard?
What is risk to people exposed?
How do we respond to the hazard?

Figure 1: Some key questions that need to be addressed when a toxic agent is released into the atmosphere.

2. General methodology

Regardless of the complexity of the dispersion models proper, the framework for estimation of expected challenge levels and the application of these challenge levels to support various CBRN defensive measures consists of three major steps as summarized in Figure 2. As is evident from this figure, the first step in the expected challenge level estimation is the hazard source characterization (cf. left-hand panel in Figure 2). This step in the process requires the detailed description of the characteristics of the source (e.g., material(s) released, location, dissemination efficiency, particle size distribution, release rate and duration, buoyancy effects due to heating or cooling at the source). For preparedness applications (which is the focus of this document), the first step involves primarily the development (formulation) of scenarios or vignettes involving the CBRN agents of interest, with the specific objective to understand the potential and specific threats (concepts of use) and, ultimately, to examine the vulnerability of a CBRN defensive system (e.g., detectors, protective clothing ensembles, medical countermeasures) to a given "attack" scenario and the likelihood that this scenario will be used by an opponent. This step of the process typically involves inputs from intelligence and threat assessments. To this purpose, hazard models can be used to assess the consequence associated with any number of hypothetical CBRN scenarios against any assumed target. The development of various scenarios provides a means to understand not only the types of CBRN threats that can potentially affect military operations, but also facilitates the determination of the potential impact of these threats on military operations and the formulation of effective countermeasures to minimize the impact.

Once the hazard source has been properly characterized, the second step in the challenge level estimation involves the utilization of an atmospheric dispersion model to predict the spread and path of the hazardous CBRN agent from the location of the release (see middle panel of Figure 2). Input to the atmospheric dispersion model will include: (1) information concerning the characteristics of the source such as the release mechanism used (e.g., spray, explosive, pyrotechnic), the nature of the source (e.g., agent released, dissemination efficiency, aerosol droplet or particle size distribution, spatial distribution of the released mass at the source), location of the release point and release rate and duration, all of which are defined in the first step of the process (cf. Figure 2), and (2) information on the local topography (terrain) and urban (building) databases, land use and land cover, and the weather conditions.

The weather data required for atmospheric dispersion models may be obtained from real-time meteorological observations, historical meteorological data, numerical weather prediction models, or simply from idealized model atmospheres (e.g., a mixed layer, stable boundary layer) with a prescribed wind speed and direction at a given height above the ground surface.

Which source of weather data is used will depend on the specific application (e.g., is the application of the methodology associated with a pre-incident planning and preparation phase, an incident response phase, or post-incident recovery phase?).

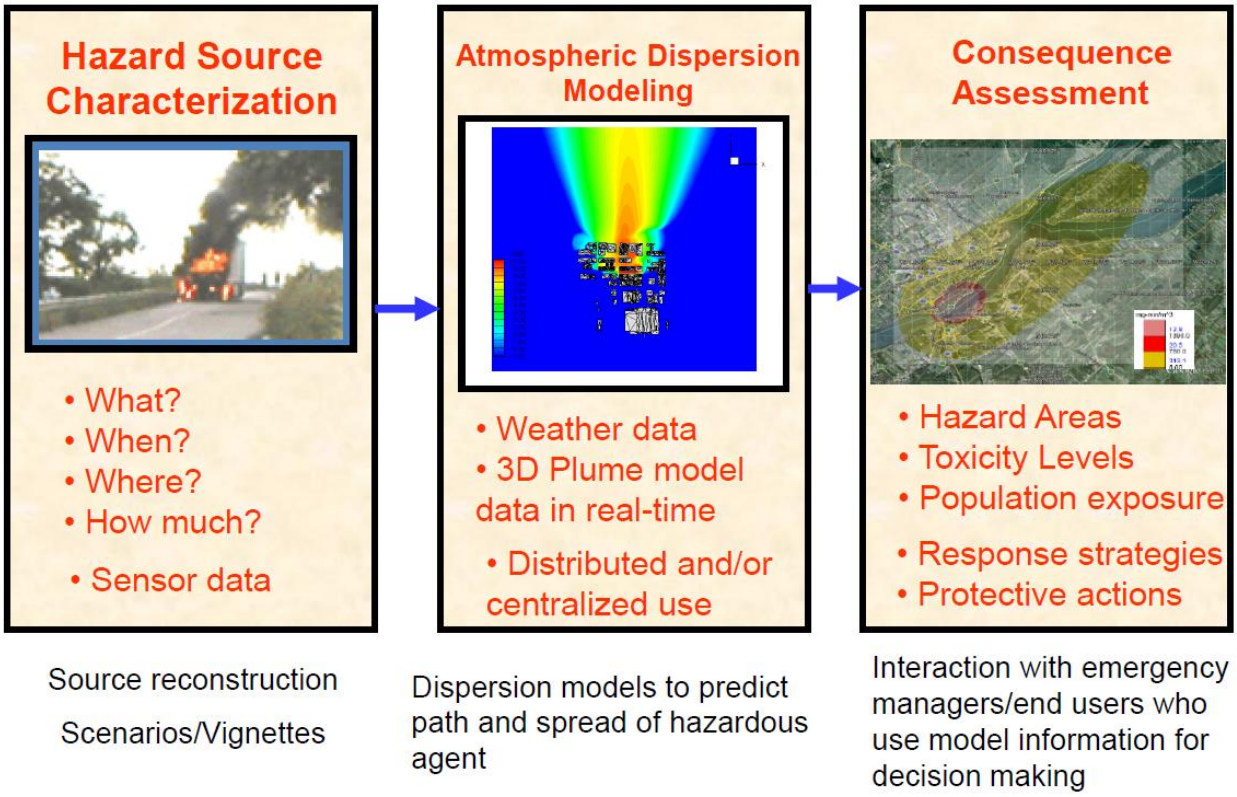

Figure 2: Three major steps in the general framework for the estimation of expected challenge levels to support CBRN defensive measures.

The atmospheric dispersion model proper provides predictions for the transport and diffusion of the toxic agent CBRN plume material in four dimensions (viz., the three dimensions of space and one of time) in the form of the concentration distribution in space-time. Various types of challenge levels extracted from this information (e.g., point concentration, partial point dosage, path-integrated concentration, ground deposition, etc. at various times and receptor locations downwind of the source position) provide the critical information on the strength (magnitude) and the extent of the CBRN hazard, as well as when and how they affect the area of military operations. This information can be utilized in the third step of the general framework for expected challenge level estimation – namely, the consequence assessment which focuses on the effects that are most likely to do the greatest harm to the exposed personnel and the impacts that these hazards will have on the area of military operations (cf. right-hand panel in Figure 2).

Consequence assessment uses challenge levels obtained in the second step (atmospheric dispersion modeling) to describe specific responses and/or effects of various military assets (e.g., receptors such as exposed personnel, detection equipment, protection equipment) and their implications and impact on military operations. The information obtained here can be used for various purposes including the formulation of appropriate tactics, techniques and procedures (TTPs) to improve operational and protective responses to CBRN incidents (in terms of response strategies, protective actions, doctrine development), decision-making for the procurement of CBRN defensive (detection and protection) equipment and for the allocation of resources (e.g., for monitoring, surveillance) and the deployment of field personnel, and generally to improve situational awareness when operating in the complex and ever changing CBRN environment. It should be emphasized that the third step of the expected challenge level estimation usually requires the determination of the response of a particular type of receptor to the expected challenge levels (e.g., point concentration, path-integrated concentration, dosage, ground deposition) determined in the second step and, as such, will necessarily require specific models for these particular types of receptors (e.g., point sensors, standoff detectors, detectors for ground and surface contamination, protective equipment, human form).

To illustrate a specific application of the general framework for the estimation of expected challenge levels shown in Figure 2, we apply it to an explicit example involving the determination of the non-inhalational (percutaneous) exposure of both unprotected and protected personnel to the release of a hypothetical very low volatility chemical warfare agent. To this purpose, all three steps in the general framework for challenge level estimation will be illustrated in detail using the example below.

3. Example

3.1 Hazard source characterization (scenario development)

The example considered herein (for illustration purposes only) concerns the determination of the expected challenge levels posed by the atmospheric release of a hypothetical chemical warfare agent having a low volatility. This hypothetical low-volatility agent (LVA) is used here only to illustrate the three key steps that need to be conducted in order to provide an estimation of expected challenge levels, in accordance to the general framework summarized in Figure 2. For this purpose, this hypothetical LVA is assumed to have the following physical and toxicological characteristics: (1) all the physical properties of the agent (e.g., surface tension, viscosity, density) are assumed to be identical to those of the classical persistent chemical

warfare nerve agent VX[1], except for the vapor pressure (or, volatility); (2) the vapor pressure of the hypothetical chemical agent is assumed to be 1/10 that of VX at any given temperature; and, (3) the hypothetical agent has a toxicity that is comparable to that of VX. Based on these assumptions, the vapor pressure of this hypothetical LVA is 3.29×10^{-5} mm Hg at 20 °C. This is about 530,000 times less volatile than water at the same temperature.

For the current scenario involving the hypothetical LVA, we consider a spray release of the agent from a single point location. The atmospheric dispersion of the windborne toxic agent material (consisting of liquid aerosol droplets and vapor) will result in both an inhalational and a non-inhalational (percutaneous) exposure on unprotected personnel located downwind of the release. The inhalational hazard consists of the primary vapor and/or the airborne liquid aerosol droplets that are small enough to be inhalable. In addition, an inhalational hazard also arises from the secondary vapor that subsequently evaporates from the liquid agent that has been deposited on the ground surface. The non-inhalational hazard results from the direct deposition of the liquid aerosol droplets in the dispersing airborne toxic cloud on the body surface of the human or from contact with the ground surface contaminated with the liquid agent.

The delivery of a chemical agent to its intended target through a spray release depends on a number of factors such as the particle size distribution, the volume application rate, and the background meteorological conditions (e.g., wind speed and direction, temperature, stability of the atmosphere, relative humidity). However, of these various factors, the one of greatest importance is the particle (or, droplet) size distribution which effectively determines the nature of the spray and how far the toxic agent cloud will "drift" downwind.

The characteristics of the spray release are determined principally by the atomization properties of the spray nozzle (or, atomizer) and by the physical characteristics of the liquid agent (e.g., surface tension, viscosity, density). In particular, the spray nozzle properties determine principally the nature of the droplet size distribution. For the current scenario involving the spray release of a hypothetical LVA, we are interested in an atomizer that is capable of providing a "fog" with liquid aerosol droplets ranging in diameter from about 1 to 30 μm. The airborne dissemination of aerosol droplet sizes in this range will result in a significant downwind atmospheric transport and diffusion of the material (e.g., over downwind distances of 10 kilometers or larger depending on the ambient meteorological conditions). On the other hand, liquid aerosol droplets that are larger than about 100 μm are subject to very short-range

[1] O-ethyl S-[2(diisopropylamino)ethyl]methylphosphonothioate

dispersion. These droplets will be strongly influenced primarily by gravitational settling to give a significant ground deposition with minimal atmospheric downwind transport and diffusion (implying, as such, very limited downwind hazard distances).

Are there atomisers that can produce a "fog" of liquid aerosol droplets in the appropriate size range so as to result in a significant downwind hazard range when the toxic agent is released into the atmosphere? A study conducted by Hoffman et al. [1] measured the atomization characteristics for four different commercially available sprayers. An important conclusion of this interesting study was that of the four sprayers that were tested, only the Colt ULV aerosol generator[2] was found to give a particle (droplet) size distribution that was consistent with that claimed by the company. More importantly, the design of the spray nozzle for the Colt ULV sprayer was such that it produced a "fog" of liquid aerosol droplets with sizes primarily in the diameter range from about 1 to 30 µm. For the current example, the droplet size distribution for the spray release of the hypothetical LVA is assumed to be similar to that which would have been obtained from the use of a Colt ULV aerosol generator. For modeling purposes, this droplet size distribution was represented analytically using a lognormal distribution. In consequence, the volume (or, mass) droplet size distribution was approximated here as a lognormal distribution with the following parameters: namely, the mass median diameter (MMD) has a value of $d_{g,v} = 15.0$ µm and the geometric standard deviation (GSD) has a value of $\sigma_g = 1.7$. This choice of MMD and GSD was found to give a very good representation for the volume droplet size distribution reported for the Colt ULV aerosol generator. More specifically, the lognormal distribution here predicts that $d_{p,10} = 8.9$ µm, $d_{p,50} = 15.0$ µm, and $d_{p,90} = 25.2$ µm. This compares to the corresponding measured values for the Colt ULV aerosol generator [1] of $d_{p,10} = 9.6 \pm 1.6$ µm, $d_{p,50} = 14.9 \pm 0.6$ µm, and $d_{p,90} = 23.3 \pm 3.0$ µm, respectively (with the reported uncertainty here corresponding to one standard deviation). Here, $d_{p,\alpha}$ is used to denote the droplet size (diameter) below which α% by volume (or, mass) of the spray is contained.

3.2 Atmospheric dispersion modeling (challenge level determination)

The second step of the general framework for challenge level estimation involves the application of an atmospheric dispersion model (see Figure 2) to determine the expected challenge levels proper arising from the release of the hypothetical LVA into the turbulent atmosphere (where the specification of this release has been determined in the first stage of the general framework as described for this example in Section 3.1 above). Various types of the

[2] The Colt ULV aerosol generated is manufactured by London Fog Inc. (Long Lake, MN).

challenge levels proper include estimates of the concentration, dosage and ground deposition of the agent as a function of location and time from a source with known emission characteristics. Which particular type of challenge level is of interest depends on the specific application (consequence assessment).

In practice, the determination of the challenge levels proper involves four parts, which are not necessarily independent of each other. These four parts are as follows: (1) specification of the properties of the initial agent cloud released into the atmosphere, before it has been transported downwind by the background meteorology; (2) definition of the properties of the model atmosphere such as the distribution of the wind speed and direction and statistics of the turbulence, as well as the topography and land use/land cover through and over which the toxic agent disperses; (3) calculation of the atmospheric dispersion of the toxic agent; and, (4) inclusion of the effects of various sources and sinks that exist in the problem (including processes such as wet deposition, dry deposition, secondary evaporation, and resuspension which accompany the agent dispersion proper). Atmospheric dispersion models have been developed in recent years to calculate the transport, diffusion and deposition of a toxic agent released into the atmosphere.

For the purposes of this example, the atmospheric transport and diffusion of the hypothetical LVA (required for the estimation of the challenge levels) will be conducted using the Hazard Prediction and Assessment Capability (HPAC) Modeling System [2]. The HPAC output corresponds to a "best estimate" for the prediction of the hazard (or, challenge level) resulting from the release of the toxic agent in terms of both the hazard evolution in time and of its location and coverage. The Analytical Incident Tool in HPAC was used to build the spray release of the hypothetical LVA described above. A material file for the hypothetical LVA was constructed for this example (see Section 3.1 for material properties for this hypothetical LVA). Sampler files were generated (for this example) in order to extract the time histories of the challenge levels in the form of the point concentration, point (partial) dosage, and path-integrated concentration for both the vapor and the liquid aerosol components at a set of pre-defined receptor locations. Finally, a meteorological scenario file for a particular model atmosphere was constructed.

The model atmosphere used for this example consists of a near-neutral atmospheric condition. In open country, this condition corresponds to at least a moderate wind speed and to a generally overcast condition (a thoroughly cloudy sky) and can be associated with either a nighttime or a daytime release. The surface roughness z_0 of the terrain over which the dispersion occurred is assumed to be 0.01 m. This surface roughness length corresponds to either grassland or cropland. For this model atmosphere, we assumed that the Monin-Obukhov length L has a value of -1000 m. The height of the atmospheric boundary layer z_i is 800 m.

The average wind speed at 10 m above the ground surface for this example is taken to be 4.0 m s^{-1}. This implies a value for the friction velocity of $u_* = 0.23$ m s^{-1}.

The hypothetical LVA agent cloud is assumed to be released into the model atmosphere using a sprayer whose characteristics have already been specified in Section 3.1 as part of the hazard source characterization. This atmosphere is assumed to be characterized by a horizontally homogeneous mean wind with turbulence statistics that are assumed to be fully developed over the level and unobstructed terrain (open country). The scenario for this example (described in Section 3.1) involves the spray dissemination of a hypothetical LVA from a localized source with a total release mass of Q kg. This release mass is interpreted to correspond to the actual mass of material that is released into the atmosphere. This is the material that will be available for the effective downwind dispersion of the toxic agent in the atmosphere. The release mass Q here is generally less than the total toxic agent mass that is contained in the sprayer. All sprayers have dissemination efficiencies that are necessarily less than the ideal of 100%. Consequently, some of the toxic agent is lost as part of the dissemination process from the sprayer. The point source used to represent the sprayer is assumed to be located 1.0 m above the ground surface. The release time for the spray dissemination is assumed to be 300 s. The initial plume size for the spray release is assumed to be 0.5 m in the two spanwise directions that are orthogonal to the downwind direction (viz., in the crosswind (or, y) and in the vertical (or, z) directions).

The expected challenge levels computed for this example (as an illustration of the types of information that can be obtained in the second step of the general framework for the estimation of challenge levels) consist of the following quantities: (1) the expected concentration C is calculated, as a function of the time t since the initial release for both the liquid aerosol and vapor components in the toxic agent cloud, at various downwind receptor locations along the plume centerline; (2) the partial dosage D is calculated as a function of the time t since the initial release for both the liquid aerosol and vapor components in the cloud at various receptor locations along the plume centerline; (3) the path-integrated concentration C_L is determined as a function of the time t since the initial release for both the liquid aerosol and vapor components in the cloud at various receptor locations along the plume centerline; (4) the ground deposition G_D and the partial dosage D are calculated as a function of the downwind distance x at various times t after the initial release; and, (5) the total surface dosage at a fixed time t after the initial release is determined.

The challenge levels for the spray release of the hypothetical LVA (obtained from the hazard modeling) are presented below in Figures 3 to 6. In the presentation here, the challenge levels have been normalized by the mass Q of the material released into the atmosphere for the given

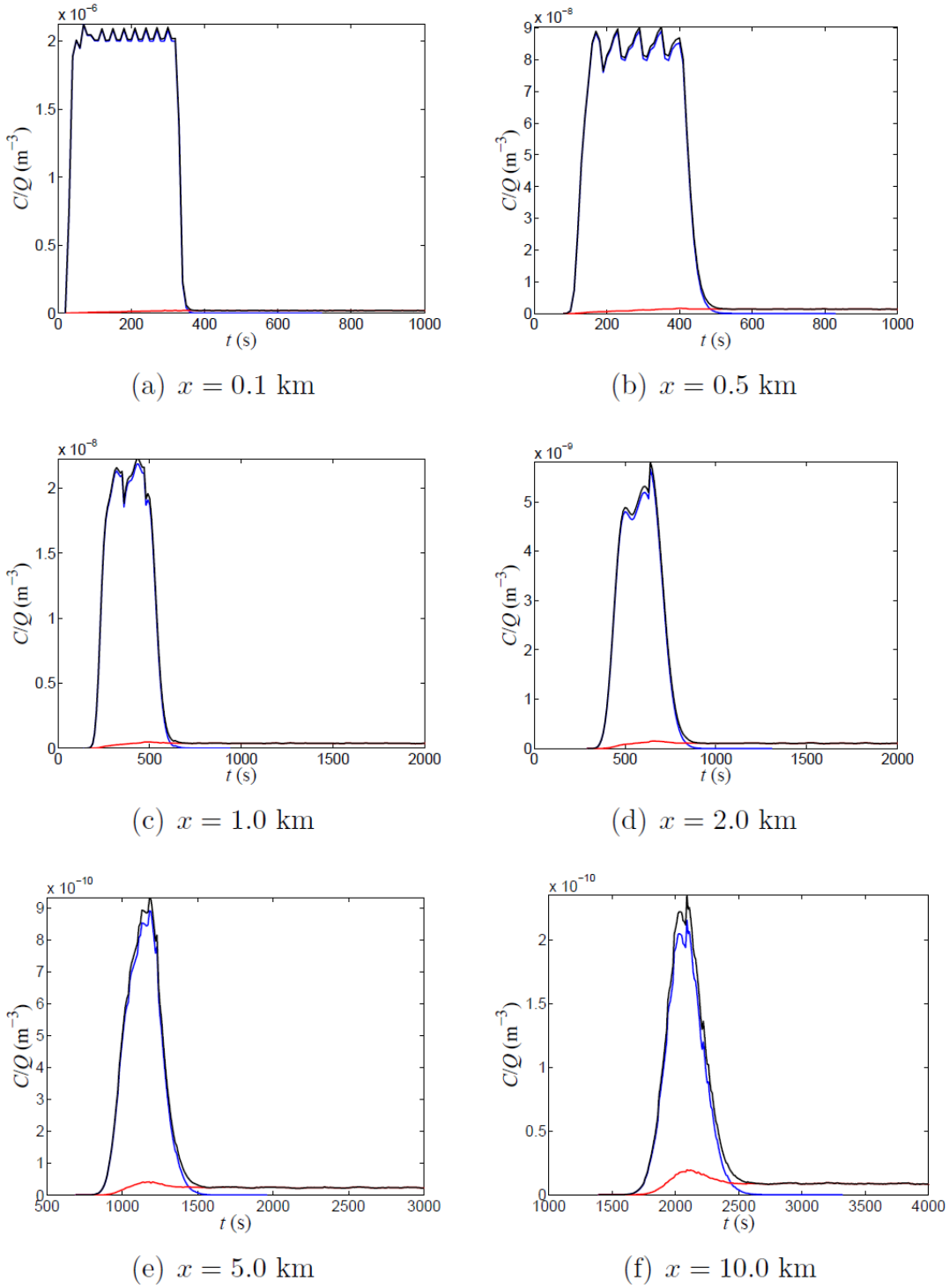

Figure 3: (a)-(f) Normalized mean concentration C/Q determined as a function of travel time t after the initial release (at $t = 0$ s) at various downwind distances x from the point source along the cloud centerline at a height of 1.7 m above the ground surface. Here, Q is the mass of LVA released into the atmosphere from the sprayer. The blue, red and black lines represent the liquid aerosol, vapor and total (sum of the liquid aerosol and vapor) concentrations C, respectively.

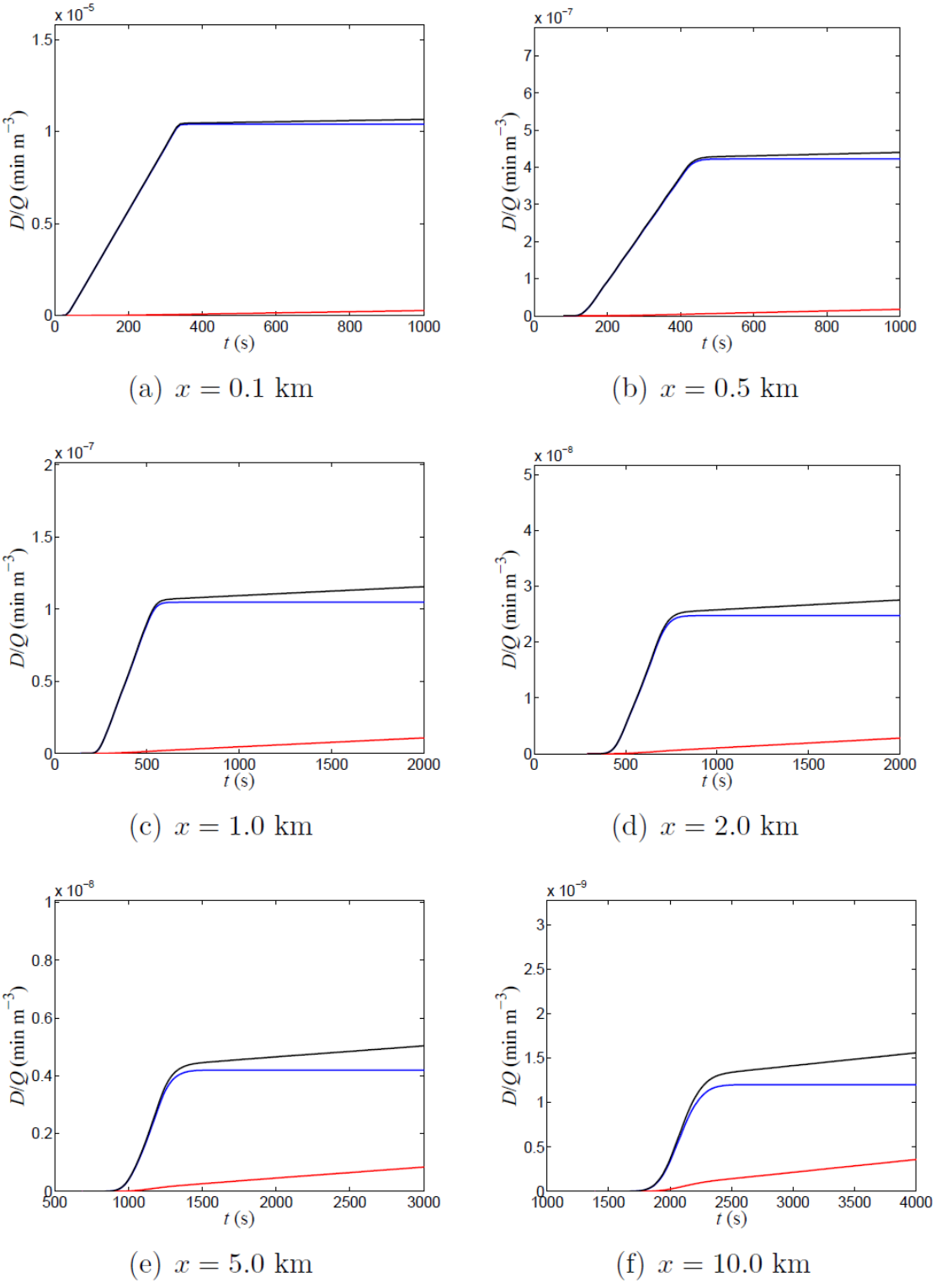

Figure 4: (a)-(f) Normalized partial dosage D/Q as a function of travel time t after the initial release (at $t = 0$ s) at various downwind distances x from the point source location along the cloud centerline at a height of 1.7 m above the ground surface. Here, Q is the mass of LVA released into the atmosphere from the sprayer. The blue, red and black lines represent the liquid aerosol, vapor and total (sum of the liquid aerosol and vapor) dosages D, respectively.

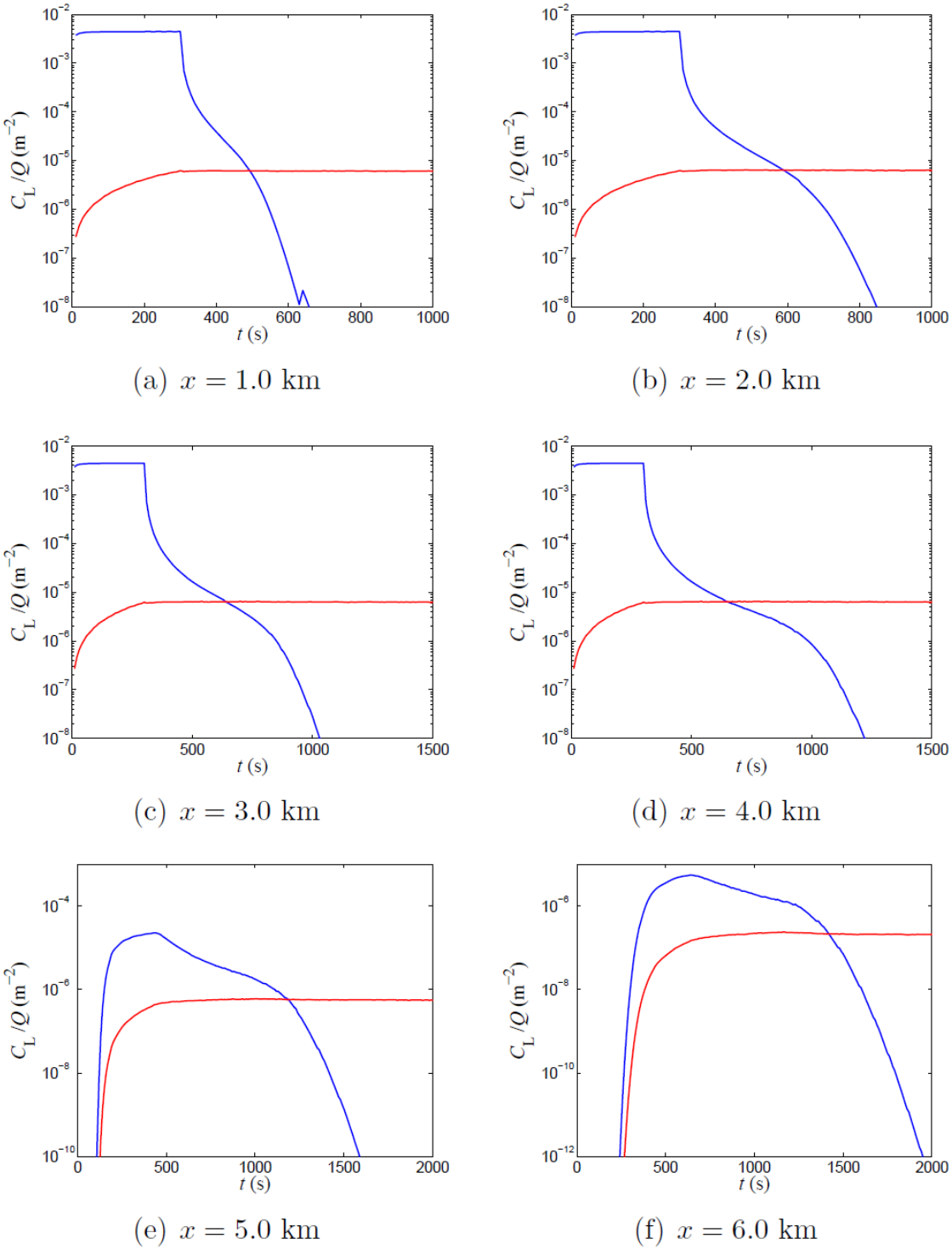

Figure 5: Normalized path-integrated concentration C_L/Q as a function of travel time t after the initial release (at $t = 0$ s) at various downwind distances x from the point source location along the cloud centerline at a height of 1.5 m above the ground surface. Here, Q is the mass of LVA released into the atmosphere from the sprayer. The blue and red lines represent the liquid aerosol and vapor components, respectively, of the path-integrated concentration C_L.

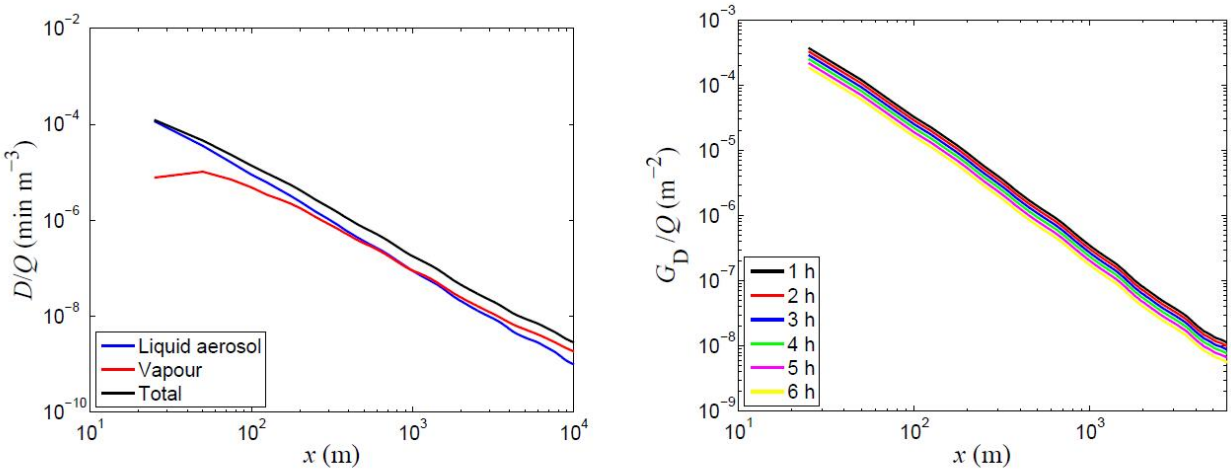

(a) Dosage (b) Ground deposition

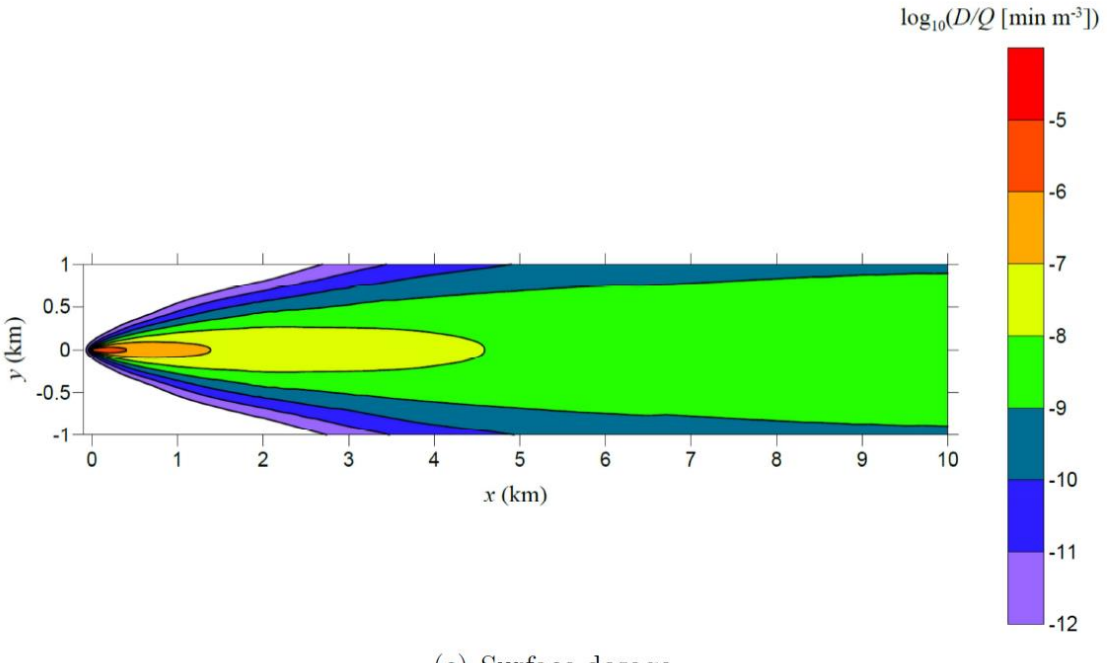

(c) Surface dosage

Figure 6: (a) Streamwise (or, alongwind) profile of the normalized partial dosage D/Q along the cloud centerline at the travel time $t = 6$ h after the initial release at a height of 1.7 m above the ground surface; (b) streamwise profile of the normalized ground deposition G_D/Q along the cloud centerline at six different travel times t after the initial release; and, (c) contours of the normalized total dosage D/Q (sum of the liquid aerosol and vapor components) obtained at ground level at a travel time $t = 6$ h after the initial release. Here, Q is the mass of LVA released into the atmosphere from the sprayer.

scenario. In particular, Figures 3 and 4 exhibit the downstream evolution of the normalized mean concentration C/Q and of the normalized partial dosage D/Q, respectively, for downwind fetches from 0.1 km to 10.0 km inclusive. In the concentration-time histories, shown

in Figure 3, the effects of the finite release duration of the sprayer (viz., 300 s) are clearly "stamped" on the concentration-time histories (at least for receptors that are less than about 500 m downwind of the source which correspond to travel times from the source to the receptor that are less than or comparable to the spray release duration). At longer downwind ranges (associated with travel times from the source to the receptor that are significantly longer than the spray release duration), the concentration-time profiles have a left-skewed Gaussian-like form (with a long trailing tail) that is more characteristic of a near-instantaneous release.

At any fixed receptor location, it can seen from Figures 3 and 4 that for the time interval associated with the complete passage of the primary cloud over the receptor, the contribution of the vapor component of the total concentration is significantly less than that of the liquid aerosol component (at least for the range of downwind distances exhibited in these figures). However, the ratio of the liquid aerosol concentration to the vapor concentration decreases monotonically with increasing downwind distance x from the source.

A perusal of either Figure 3 or 4 shows that at any fixed receptor, the concentration C is nonzero even long after the passage of the primary cloud consisting of the windborne liquid aerosol droplets and the primary vapor (viz., evaporation of the material from the airborne droplets). The concentration C that persists after the passage of the primary cloud consists entirely of the toxic agent vapor (see the red curves in Figures 3 or 4) and arises entirely from the surface evaporation and subsequent diffusion of the secondary vapor from the contaminated ground cover. The normalized ground deposition density G_D/Q computed as a function of the downwind distance x along the cloud centerline is displayed in Figure 6(b) for six different times t after the initial spray release. Interestingly, the ground deposition for this example shows a power-law variation as a function of the downwind distance x from the source. In other words, $G_D \propto x^{-p}$ for some (decay) exponent $p > 0$ over the available downwind fetch shown in Figure 6(b). Furthermore, it is seen that at each downwind distance, the rate of the surface evaporation is equal (approximately or better). This fact follows directly from the observation that the curves for G_D/Q exhibited in Figure 6(b) are approximately parallel to each other for the six different times shown.

Figure 5 exhibits the path-integrated concentration C_L/Q at six different receptor locations downwind of the source. For the purposes of this example, the path-integrated concentration has been obtained for a line of sight that is oriented horizontally and directed upwind through the central core of the approaching toxic agent cloud at a height of 1.5 m above the ground surface providing, as such, the expected maximum values of C_L through the cloud at any time t after the release. It is evident that the contribution to C_L from the vapor component is smaller than that from the liquid aerosol component, at least for travel times t associated approximately with the arrival of the leading (or, front) edge of the cloud at a given receptor location. At longer travel times, the liquid aerosol contribution to C_L is smaller than that of the vapor contribution. It is noted that the vapor component of C_L is approximately constant. This constant component arises entirely from the secondary evaporation of the toxic agent from the contaminated ground cover.

The finite duration of the spray release is "stamped" also in the path-integrated concentration time history for receptors that are located up to about 4.0 km downwind of the spray release (see Figure 5). From Figure 5, it is evident that for those receptors that are located at $x = 1$, 2, 3 and 4 km downwind of the source, after the end of the spray release (viz., at 300 s after the initial release), the path-integrated concentration C_L associated with the liquid aerosol droplet contribution is a generally monotonically decreasing function of the time t. Two rates of decrease are apparent in the time history of C_L: namely, one rate is associated with the early phase of the dispersion and another rate is associated with the late phase of the dispersion, where the "early" and "late" are used as descriptors of travel times that are small or large, respectively, with respect to a reference time associated with the arrival of the front (or, leading) edge of the toxic agent cloud at the given receptor location. The rate of decrease of C_L in the early phase of dispersion corresponds to the situation where the leading or front edge of the dispersing toxic agent cloud is upwind of the receptor location. This rate of decrease is slower than the rate of decrease of C_L associated with the late phase of dispersion. The latter corresponds to the situation when the front edge of the cloud has already advected past the receptor location.

For receptor locations at $x = 5$ and 6 km downwind of the spray release (see Figure 5), it is noted that the dispersing toxic agent cloud initially lies beyond the event horizon for the receptor (viz., the cloud is located initially beyond the horizon along the specified line of sight used to calculate the path-integrated concentration[3]). As a result, for an initial duration associated with the early phase of dispersion for these receptors, the cloud is located outside the event horizon, with the result that $C_L = 0$ for the liquid aerosol and vapor components of the primary cloud. Once the front edge of the approaching cloud appears within the event horizon for the given receptor location, the path-integrated concentration is seen to increase rapidly to a maximum value. This maximum value corresponds to the time $t = t_*$ when the entire cloud lies within the event horizon associated with the receptor location. After the time $t = t_*$, the temporal evolution of C_L is seen to resemble that observed for the receptor locations at $x = 1$, 2, 3, and 4 km from the source at times after it has been switched off. In particular, note that for the receptor locations at $x = 5$ and 6 km, C_L for the liquid aerosol contribution decreases monotonically with time t for $t > t_*$, exhibiting two distinct rates of decrease associated, as such, with the early and late phases of dispersion. These were also observed for the receptors closer to the release location [see Figures 5(a)-(d)].

3.3 Consequence assessment

The third step of the general framework for challenge level estimation (see Figure 2) involves the use of the challenge levels determined in the second stage of the framework to conduct some form of consequence assessment. Generally, the nature of this assessment is to answer

[3] Indeed, for a line of sight directed upwind at a height of 1.5 m above the ground surface, the distance to the horizon over open and unobstructed terrain is about 4,374 m.

or address some specific question or problem. The information embodied in the expected challenge levels extracted in the second step can be used for consequence assessment and for determination of the requirements for detection and protection (against the challenge). For example, the total dosage (sum of the liquid aerosol droplet and vapor contributions) when used in conjunction with supplementary information concerning the acute inhalation toxicology of the LVA can be used to assess the expected toxicological effects (injury and lethality) in the exposed military population arising from the inhalational exposure to the toxic agent. The point concentration time histories of the liquid aerosol droplet component of the primary toxic agent cloud can be used to assess the non-inhalational (or, percutaneous) exposure of either unprotected or protected personnel to the agent.

The mean concentration C and the path-integrated concentration C_L can be used to assess the detection performance of or to develop requirements for existing (in-service) or next-generation chemical sensor systems against putative toxic agent challenges for, respectively, point and standoff detection when applied in a "detect to protect" or in a "detect to warn" paradigm, respectively. Furthermore, the ground deposition G_D can be used to assess the performance of or requirements for either in-service or proposed chemical sensing technologies for the detection and mapping of toxic agent ground contamination. As a specific example of the application of challenge levels, models for light scattering by airborne particulates (aerosol droplets) using the theory for atmospheric radiative transfer can be used in conjunction with specific standoff sensor models and the path-integrated concentration C_L (liquid aerosol droplet and vapor components) determined in Section 3.2 to assess or to define requirements for the detection performance of either in-service or proposed next-generation standoff chemical detection systems.

Each application of the challenge levels noted above requires one to determine how a specific instantiation of a receptor (e.g., chemical detector, exposed personnel in unprotected or protected posture, etc.) will respond to the challenge levels (e.g., point concentration, path-integrated concentration, ground deposition, etc.) or, equivalently, how the challenge levels will affect the receptor. To illustrate the third step of the general framework for expected challenge level estimation, let us continue with our example and consider the following application: determine the non-inhalational (percutaneous) exposure of unprotected and protected personnel at a specified receptor location downwind of the spray release of the hypothetical LVA. To accomplish this, one needs to account properly for the complexity of the highly disturbed flow in and around the human form, which determines ultimately the necessarily complex pattern of aerosol deposition on the surface of the human body. The deposition of the LVA droplets (particulates) on surface of the human body originates from many factors including gravitational sedimentation, the weight or inertia of the droplets, molecular and turbulent diffusion, and nature of the impingement on the body from the disturbed (swirling) moving air in the complex flow field around the human form.

Cloud transport and diffusion models have evolved substantially in recent years, making available such tools as the HPAC model which is well-suited for predicting the large-scale transport and diffusion of toxic agent material in the atmosphere. However, for small-scale

problems such as surface deposition onto the human form, it is appropriate to incorporate local transport effects attributable to droplet mass (or, size) as well as other processes such as aerodynamic drag. This information is embodied in the collection (or trapping) efficiency of the human form when placed in the path of a challenge liquid aerosol stream, defined simply as the amount of particulates of a given size (diameter) actually impacting on any portion of the human body relative to the amount which would pass through its projected area if it were removed. The calculations required to determine the trapping efficiency of the human form for a challenge aerosol concentration are illustrated in Figure 7.

Firstly, we require a realistic and accurate representation of the human form. To that end, the geometry of a computerized manikin used for this example corresponds to a realistic and accurate representation of a nude standing male figure with arms spread (cf. lower portion of Figure 7). This male figure has a height of 1.8 m, with a corresponding body surface area of 1.85 m^2. The geometry of the human form is extremely complex and, as a result, a high-fidelity digitization of the form is a challenging problem. The accuracy of the detailed modeling of the disturbed flow around the human form depends critically on the quality of this digitization (discrete representation). To this purpose, the surface of the human form has been represented using 89,360 nodes (points) and a corresponding connectivity list. This list provides information on how these nodes are connected together to form 178,716 triangular elements (or, patches) that provide an accurate representation for the surface of the human body.

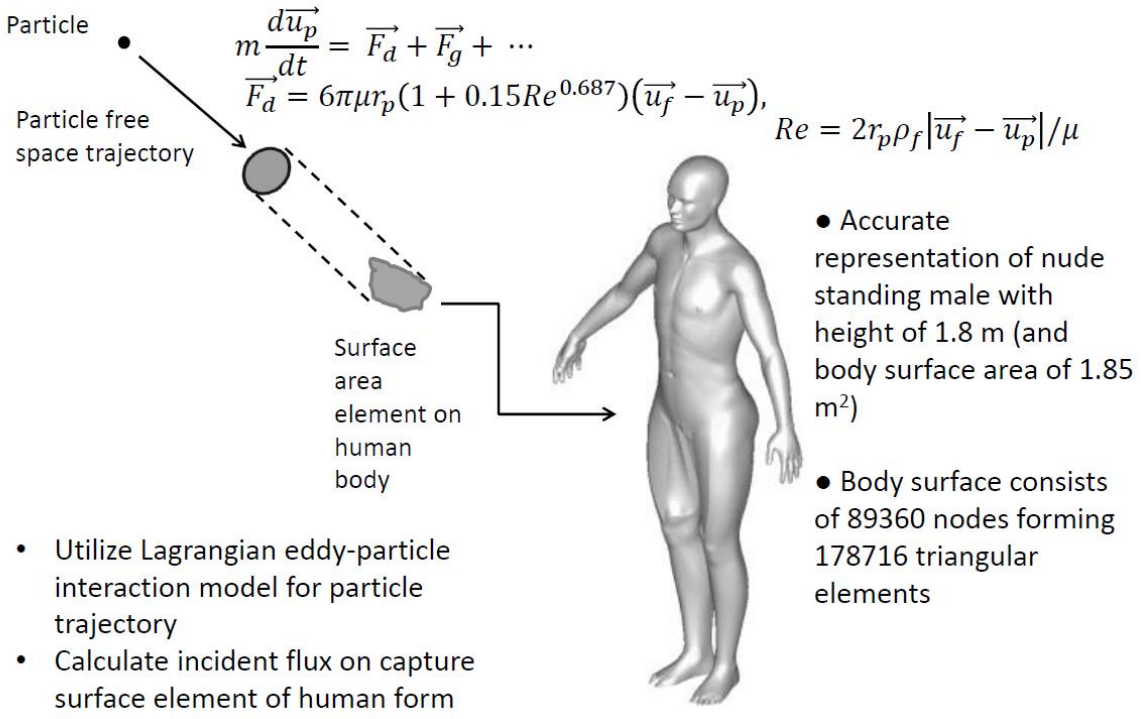

Figure 7: The steps used for the determination of the trapping (collection) efficiency of the human form placed in the path of a challenge aerosol concentration.

Secondly, the prediction of the aerosol particulate (droplet) dispersion and possible deposition on the surface of the human body (computational manikin) involves numerically tracking particles released just upwind of the human body into the highly disturbed turbulent flow in the vicinity of and around this complex form. The trajectory of the discrete phase particle is tracked by integrating the force balance (Newton's second law of motion) on the particle which is written in a Lagrangian reference frame. Drag, gravitational settling, Saffman lift force, electrostatic force, and turbulent and Brownian diffusions can all be considered in the process of this computation. However, for the case in this example which involves droplet sizes (diameters) that are of the order of one micron or larger, the principal (or major) forces acting on the droplet are the aerodynamic drag force and the gravitational settling force (assuming implicitly that the particle and the human body are electrically neutral, so no electrostatic attractive or repulsive forces). With this simplification, Newton's second law of motion that determines the trajectory of the droplets can be written as (cf. upper left portion of Figure 7)

$$\left(\frac{4}{3}\pi r_p^3\right)\rho_p \frac{d\vec{u}_p}{dt} = \vec{F}_d + \vec{F}_g \,, \tag{1}$$

where $\vec{F}_d$ is the drag force and $\vec{F}_g$ is the gravitational settling force acting on the particle. The drag force is parameterized using Stokes linear resistance form for parameterization of the drag coefficient and assumes the following form:

$$\vec{F}_d = 6\pi\mu r_p(1 + 0.15Re^{0.687})\left(\vec{u}_f - \vec{u}_p\right).$$

Here, $\vec{u}_f$ is the (instantaneous) fluid phase velocity, $\vec{u}_p$ is the discrete phase particle velocity, μ is the dynamic viscosity of the fluid (air), r_p is the particle radius, and Re is the relative Reynolds number defined as follows:

$$Re = \frac{2r_p\rho_f\left|\vec{u}_f - \vec{u}_p\right|}{\mu} \,,$$

where ρ_f is the density of the fluid and $|\vec{s}|$ denotes the Euclidean length of the vector $\vec{s}$. Finally, the term $\vec{F}_g \stackrel{\text{def}}{=} {}^4\!/_3\,\pi r_p^3\left(\rho_p - \rho_f\right)\vec{g}$ is the gravitational settling term where ρ_p is the particle density and $\vec{g}$ is the gravitational acceleration vector. The particle equations of motion are discretized and solved numerically using a first-order time-stepping scheme in order to calculate the incident flux of particles on the various surface elements (patches) that comprise the human form. From this information, the trapping efficiency (or, deposition probability) of the challenge aerosol droplets of a given size (diameter) can be determined at each location (or surface patch) of the human form.

Thirdly, it is noted that the determination of the trapping efficiency (deposition probability) requires a knowledge of the fluid phase velocity $\vec{u}_f$ around the human form. Indeed, a proper representation of the highly disturbed complex flow around the human form (primary flow)

is crucial for the accurate prediction of the deposition rate of particulates on the surface of the human body. To this purpose, the mean flow and the turbulence kinetic energy around the human form were obtained using the Reynolds-averaged Navier-Stokes (RANS) equations, in conjunction with a conventional k-ε turbulence closure model. Practically speaking, the strategy is computationally efficient and is to be preferred for the prediction of the flow around the human body[4]. In RANS, the flow variables (such as velocity and pressure) are decomposed into a mean component and a fluctuating component. The mean velocity field and the pressure are obtained by solving the continuity and RANS equations, whereas the turbulence closure model is used to obtain the statistics of the fluctuating velocity which is not resolved explicitly in the computations.

It is noted that the RANS approach only provides the highly disturbed mean velocity field of the flow around and in the vicinity of the human form. The prediction of the trapping efficiency on the surface of the human body requires a knowledge of the instantaneous fluid phase velocity. Towards this purpose, the eddy-interaction model (EIM) is used in conjunction with the mean velocity field of the fluid provided by the RANS model in order to determine the trapping efficiency. In EIM, a particle is allowed to interact successively with various eddies in the flow. Each eddy has a characteristic lifetime, length and velocity scales that are obtained from the primary flow calculation results using the RANS model with an appropriate turbulence closure. The end of the interaction between a particle and one eddy occurs when the lifetime of the eddy is over or when the particle crosses the spatial extent of the eddy. At this instant, a new interaction for the particle with a new eddy is started. The trajectory of the particle will be determined in accordance to its equations of motion [Equation (1)]. When the particle enters the eddy, the local fluctuating velocity at the location of the particle is added to the local mean velocity (obtained from the RANS prediction) to obtain the instantaneous fluid phase velocity used in the particle equation of motion. The local fluctuating velocities are obtained by simply multiplying the root-mean-square fluid fluctuating velocities by random numbers generated from a Gaussian probability density function of zero mean and unit standard deviation at the start of one eddy-particle interaction.

In order to obtain the trapping efficiency (or, deposition probability) on various parts of the human form, hundreds of thousands to millions of particles must be released into the flow. The coupled effect of the human form and the highly disturbed primary flow are computed on a volumetric grid of points around the human body, where a Reynolds-averaged flow field is determined using the RANS methodology. The time-averaged flow field and a reconstruction of the fluctuating (turbulent) velocity components using EIM are employed to convect an array of the particles (droplets) from their starting positions on the boundary of the computational grid until they either impact the human body surface (and, hence, provide a contribution to the deposition probability in a given surface patch or element of the body surface) or encounter another boundary of the grid (at which point the particle is assumed to

[4] Direct numerical simulation and large-eddy simulation, which would be more ideal, are too computationally expensive to apply to the current problem.

have not impacted and deposited on the human form). The effective collection rate on each surface patch of the human form is used to determine the trapping efficiency for that part of the body surface.

Figure 8 displays an example of the computation of the highly disturbed velocity field around and in the vicinity of the human form for the case of the body oriented at an angle of 0° with respect to the incident wind direction. For visualization purposes, the mean flow fields and streamlines in two cross-sections through the human form are shown in this figure: namely, in a vertical x-z plane bisecting the human form along a vertical plane through the body and in a horizontal x-y plane bisecting the human form at half height. In particular, stream traces (top panels) and the velocity field components (bottom panels) along a vertical and a horizontal cross-section through the human form are exhibited in Figure 8. Superimposed in the various panels of this figure is the velocity magnitude, which has been false colored.

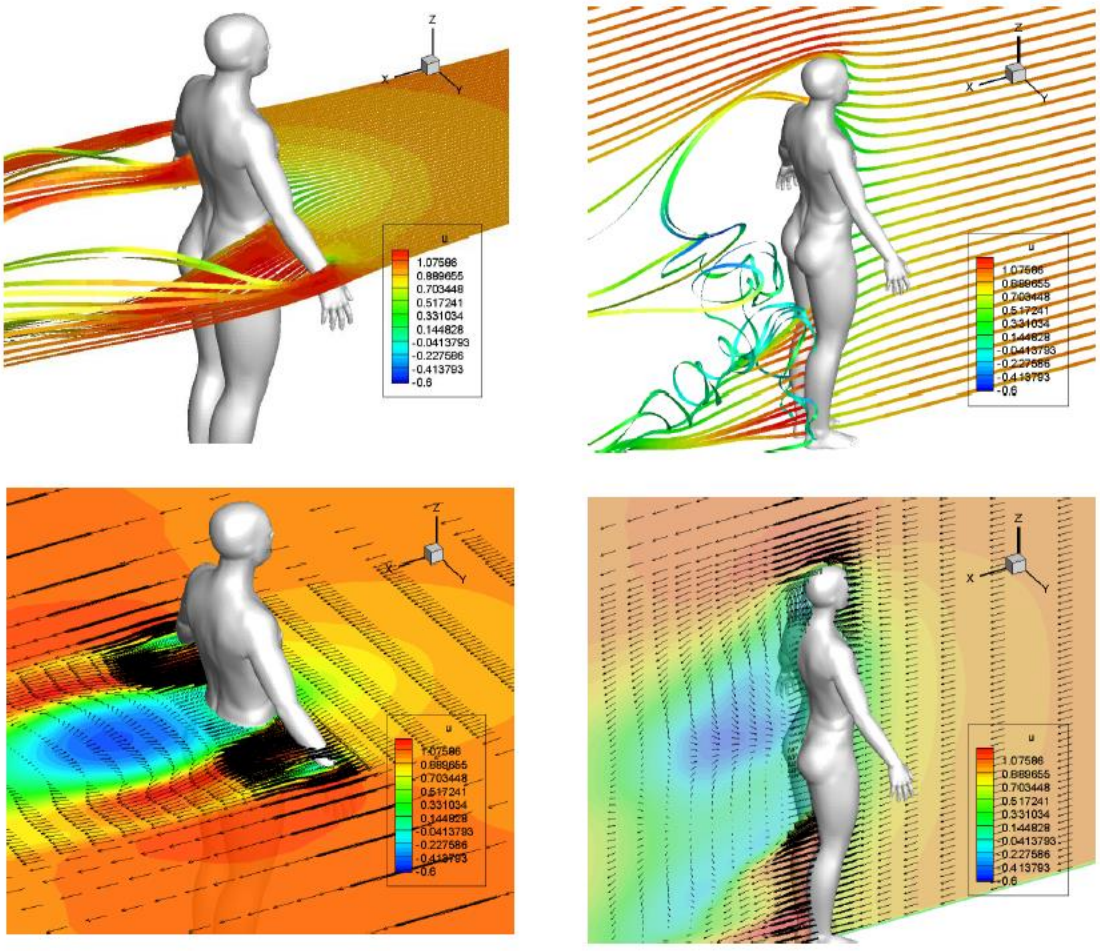

Figure 8: RANS methodology used in the prediction of the highly disturbed velocity field in and around the human form. The body is oriented at 0° with respect to the incoming (prevailing) wind direction (along the positive x axis in this example).

From Figure 8, it can be seen that complicated vortices and swirling flows are generated around and behind the human form. Of these, the streamline traces (top panels) clearly exhibit the complexity of the swirling flow and the three-dimensional vortical patterns that are generated behind the human body. There are stagnation points on the windward side of the body. The side views of the human form show the presence of two vertically stacked large counter-clockwise rotating eddies generated in the wake region of the human form. Indeed, there is a fairly large recirculation zone present in the rear of the body. This zone exhibits a strong reverse flow to the incoming (prevailing) flow. The presence of these flow features implies that any aerosol droplets (particles) that are transported downstream in the immediate vicinity of the body can potentially be entrained into the recirculating flow in the body wake region and be deposited subsequently in the rear region of the body.

Owing to the complexity of the flow in and around the human form, the pattern of aerosol deposition on the human body is generally very complicated. Figure 9 shows the complexity of this deposition pattern for the case of a person facing directly into the incoming wind (viz., 0° orientation with respect to the wind direction). The calculation here is for mono-disperse aerosol particulates (droplets) with a diameter of 1.585 μm. The distribution of the deposition probability on the surface of the human body has been estimated using 1,000,000 particles which were released uniformly in a vertical plane just upwind of the human form. Figure 9 exhibits high-resolution isopleths for the deposition probability (or, trapping efficiency). It can be seen for this specific case that the largest deposition occurs on the upper chest and abdomen as well as along the front of the arms, thighs and shins, but the nature of the three-dimensional vortical flow implies that there are localized “hot spots” of deposition along the sides and in the rear of the human form (e.g., in the small of the back and in the rear lower leg region). The nature of this deposition depends sensitively on the orientation of the human body with respect to the incident wind direction and on the aerosol particle size.

Deposition probability maps similar to Figure 9 can be computed for a range of particle sizes and this information can be used subsequently to estimate the deposition density on the surface of the human body for a given challenge level. Continuing with our current example, we have computed deposition probability maps for 13 aerosol particle size diameters. The 13 particle size diameters used for this example were equally spaced logarithmically between 0.1 and 40 μm. More specifically, the particle diameters used for the current calculation were as follows: 0.1585, 0.2511, 0.3981, 0.631, 1.0, 1.585, 2.511, 3.981, 6.31, 10.0, 15.85, 25.11, and 39.81 μm. These deposition probability maps for the surface of the human form can be used in conjunction with the challenge levels (in particular, the concentration time histories C of the liquid aerosol component) obtained at various receptor locations (see Section 3.2) to determine the deposition density on the human body, when exposed to the given challenge level in either an unprotected or protected posture. For the latter, information on the penetration probability for the protective clothing ensemble will be required also for the consequence assessment.

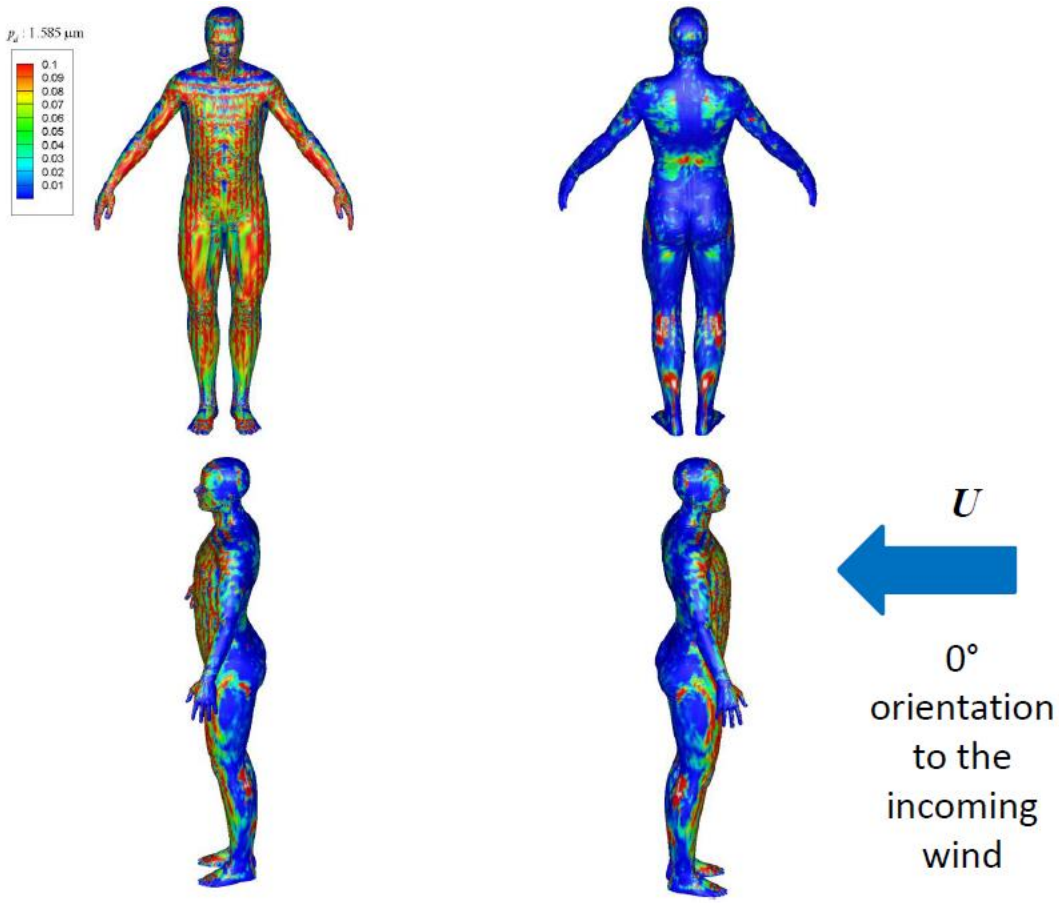

Figure 9: Front, back, left and right side views of the deposition probability (trapping efficiency) p_d of the human form for a person facing directly into the direction of the incoming wind (viz., with a 0° orientation with respect to the incoming wind). The deposition probability has been determined for aerosol particles having a diameter of 1.585 µm.

To this purpose, the information embodied in the challenge levels (point concentration-time history), in the deposition probability maps obtained as a function of the aerosol particle size (diameter), and in the time-varying droplet size distribution can now be combined to determine the deposition density on the human form for either unprotected or protected personnel (the latter of which requires also information on the penetration probability through the protective clothing ensemble). The deposition density $\rho_b(\vec{r}_b, t)$ at location $\vec{r}_b$ on the body surface and at time t after the initial release can be determined as follows:

$$\rho_b(\vec{r}_b, t) = \int_0^t UC(\vec{x}_r, t') \left(\int \tilde{\varphi}(d, t')\, p_d(\vec{r}_b|d)\gamma(d)d\log d \right) dt' \,, \qquad (2)$$

where U is the advection velocity, $C(\vec{x}_r, t')$ is the concentration at the receptor location $\vec{x}_r$ (where the person is located) at the time t' (after the initial release), $\tilde{\varphi}(d, t')$ is the particle (or,

droplet) size distribution at time t',[5] $p_d(\vec{r}_b|d)$ is the deposition probability for particles of diameter d at the body surface location $\vec{r}_b$, and $\gamma(d)$ is the penetration probability through the protective clothing ensemble for particles (droplets) of diameter d. For unprotected personnel, $\gamma(d) = 1$ for all particle diameters d. Note that $UC(\vec{x}_r, t')$ is the mass flux in a vertical plane just upstream of the human form (person) situated at the receptor location $\vec{x}_r$.

As an example of the application of Equation (2), Figure 10 displays the deposition density on the human body for a receptor that is located 2 km directly downwind of the spray release. The challenge level in the form of the point liquid aerosol concentration C was determined earlier and is shown in Figure 3(d) as the blue curve (normalized by the mass Q released by the sprayer into the atmosphere). For this challenge level, the deposition density per unit mass of material released from the source (ρ_b/Q) is displayed in Figure 10 (for an unprotected person) at a time $t = 2000$ s. This time corresponds to the entire passage of the liquid aerosol (primary) cloud at the given receptor location. Note that the deposition density pattern on the human body is extremely complex owing to the highly disturbed flow around the body. Given the deposition density on the human form for the predicted challenge level, it is now straightforward to integrate the deposition density over the surface area of each body part to obtain the deposited mass on that part per unit mass released into the atmosphere (at the source). For the unprotected person, this information is summarized for this case (cf. Figure 10) in Table 1. From the information in Table 1, it can be determined that the total mass deposited on the unprotected human body per unit mass released at the source for the liquid aerosol challenge level shown in Figure 3(d) is 3.499×10^{-7}.

The calculations of the deposition on the human form for unprotected personnel can be repeated for protected personnel. The results of this calculation are summarized in Figure 11 which displays the deposition density per unit mass released at the source for protected personnel at the same receptor location and for the same challenge levels as shown in Figure 10 for the unprotected personnel. The protective penetration probability $\gamma(d)$ is exhibited in the lower left corner (inset) in Figure 11. The penetration probability for the protective clothing ensemble was obtained from swatch tests (S. Duncan, pers. comm.) Again, from the distribution of the deposition density on the human body (underneath the protective clothing ensemble in this case), the deposited mass on each part of the body can be determined. This information is summarized in Table 2 and based on this information, it is seen that the total mass deposited on the protected human body per unit mass released at the source, for the liquid aerosol challenge level shown in Figure 3(d) and for the protective clothing ensemble with penetration probability given in the lower left inset in Figure 11, is 3.037×10^{-10}. Crudely, it is seen that this protective clothing ensemble provides a protection factor of about 1000 (based on the total mass deposited on the body over all particle sizes).

---

[5] The D^2 law (derived from hydrodynamic theory), which states that the rate of change of the square of the droplet diameter is constant, was used to approximate the time evolution of the droplet size distribution. The constant K in this law can be determined in terms of the binary diffusion coefficient of the vapor phase of the toxic agent in air, the molecular weight of the agent, the density of the toxic agent liquid droplet, the partial pressure of the vapor phase of the agent away from the droplet, the saturation partial pressure of the vapor at the droplet surface, and the surface temperature of the liquid agent droplet.

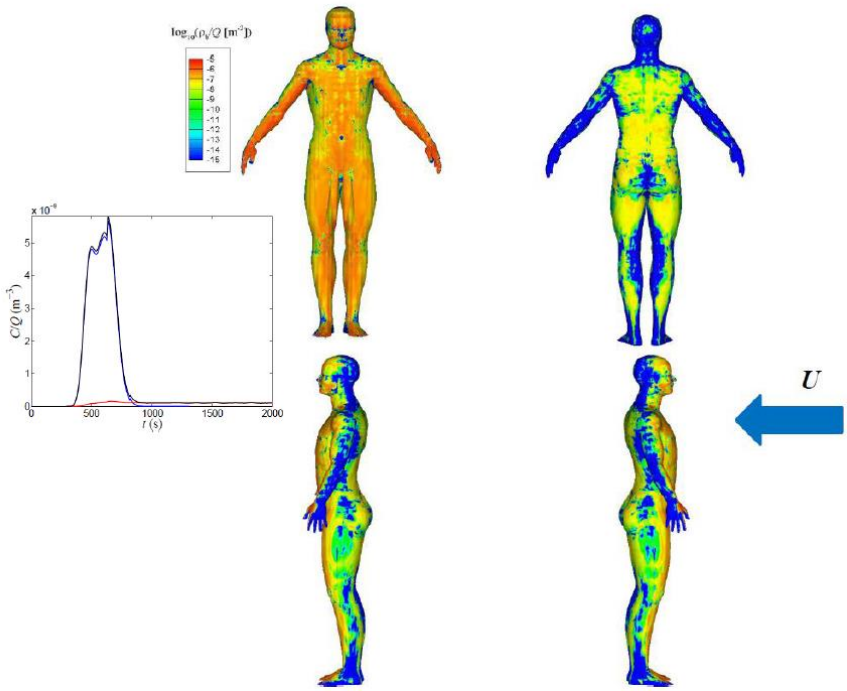

Figure 10: Distribution of the deposition density ρ_b on the unprotected human form per unit mass released into the atmosphere at the source for a receptor at a location 2 km downwind of the source. The inset (left) shows the liquid aerosol challenge level (blue line) that produced the given deposition density on the body.

Table 1: Mass deposited on various parts of the unprotected human body per unit mass released at the source for the deposition density pattern shown in Figure 10.

Body part	Deposited mass (per unit mass released)	Fractional contribution
Head (entire)	1.905×10^{-8}	0.0544
Neck (entire)	1.568×10^{-9}	0.0045
Upper chest (including shoulders)	2.830×10^{-8}	0.0809
Lower abdomen (down to waist)	2.943×10^{-8}	0.0841
Arms (left and right)	8.186×10^{-8}	0.2341
Hands (left and right)	3.555×10^{-8}	0.1016
Legs (left and right)	1.065×10^{-7}	0.3044
Feet (left and right)	2.097×10^{-8}	0.0600
Back	5.101×10^{-9}	0.0146
Buttocks	3.230×10^{-9}	0.0092
Crotch area	1.827×10^{-8}	0.0522
Total	**3.499×10^{-7}**	**1.0000**

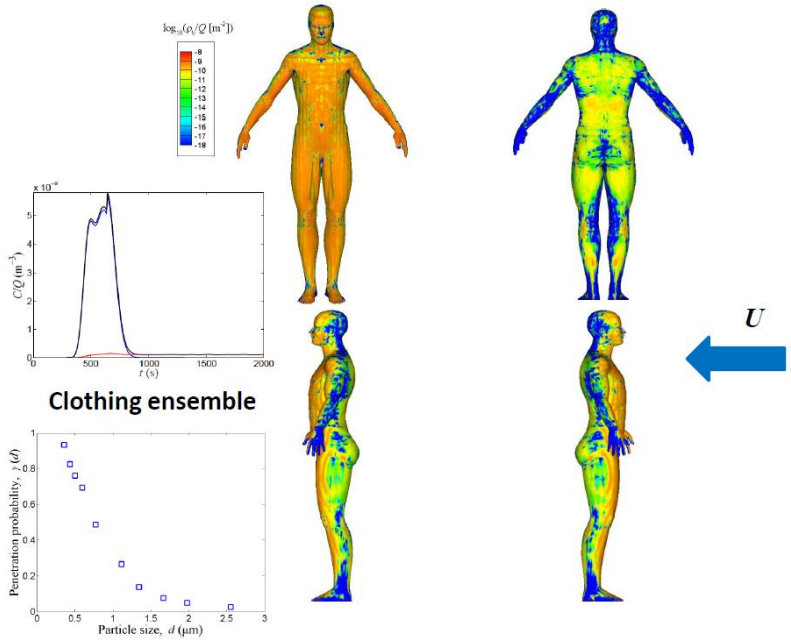

Figure 11: Distribution of the deposition density ρ_b on the protected human form per unit mass released into the atmosphere at the source for a receptor at a location 2 km downwind of the source. The insets (upper and lower left) show, respectively, the liquid aerosol challenge level that produced the given deposition density on the protected body and the penetration probability $\gamma(d)$ for the protective clothing ensemble.

Table 2: Mass deposited on various parts of the protected human body per unit mass released at the source for the deposition density pattern shown in Figure 11.

Body part	Deposited mass (per unit mass released)	Fractional contribution
Head (entire)	1.750×10^{-11}	0.0576
Neck (entire)	2.278×10^{-12}	0.0075
Upper chest (including shoulders)	2.926×10^{-11}	0.0963
Lower abdomen (down to waist)	3.836×10^{-11}	0.1264
Arms (left and right)	4.955×10^{-11}	0.1632
Hands (left and right)	1.923×10^{-11}	0.0633
Legs (left and right)	1.023×10^{-10}	0.3368
Feet (left and right)	1.546×10^{-11}	0.0510
Back	5.646×10^{-12}	0.0186
Buttocks	4.296×10^{-12}	0.0141
Crotch area	1.981×10^{-11}	0.0652
Total	**3.037×10^{-10}**	**1.0000**

From the information presented in Figures 10 and 11, as well as in Tables 1 and 2, the toxicological assessment for the non-inhalational (percutaneous) exposure to the hypothetical LVA for both unprotected and protected personnel can be obtained. To continue with our example, it will be assumed (for the purposes of this discussion) that the human estimate for the LD_{50} (viz., lethal dose that will kill 50% of the exposed population for non-inhalational or percutaneous exposure) of our hypothetical LVA is 2.0 mg/70 kg (man)[6] (or, equivalently, 0.0286 mg/kg). Using this value for the LD_{50} of our hypothetical LVA, it can be seen from Table 1 that the release of a quantity of agent $Q = 5.7$ kg into the atmosphere will result in an LD_{50} for non-inhalational exposure for an unprotected 70 kg man located 2 km downwind of the source (for the scenario considered in Section 3.1). Similarly, using the results summarized in Table 1, it can be seen that the same man wearing non-protective clothing (e.g., light battle dress or gear) with a protection factor of 25 that covers all parts of the body with the exception of the head, neck and hands will experience a non-inhalational exposure of about 0.2(LD_{50}) if $Q = 5.7$ kg of the hypothetical LVA is released into the atmosphere at the source. Finally, continuing with the toxicological assessment, the information contained in Table 2 can be used to determine that a human in the protective clothing ensemble (whose penetration probability in summarized in Figure 11) will experience a non-inhalational exposure of 8.65×10^{-4} (LD_{50}) if $Q = 5.7$ kg of the hypothetical LVA is released into the atmosphere at the source. It is assessed in this example that the protective clothing ensemble is very effective.

4. Conclusions

The three key steps in the determination of expected challenge levels for support of CBRN defensive measures have been described. These three key steps of the expected challenge level determination are: (1) hazard source characterization to define the characteristics of the source; (2) atmospheric dispersion modeling using the information in the first step (as initial/boundary conditions for the problem) to calculate various facets of the challenge level (e.g., point concentration, path-integrated concentration, dosage, ground surface deposition, etc.); and, (3) consequence assessment which utilizes the challenge levels proper determined in the second stage of the process to address various operational issues (e.g., adequacy of point or standoff detection systems, determination of the inhalational and non-inhalational exposures for unprotected and protected personnel under various scenarios, adequacy of protective clothing ensembles, development of TTPs for operating effectively in a CBRN environment, etc.). A simple example has been worked through in detail in order to illustrate these three key steps of expected challenge level estimation.

[6] This value for the LD_{50} of the hypothetical LVA for percutaneous exposure is comparable to that of VX.

In this report, the three key steps of the expected challenge level estimation schema have focused on an application in a pre-incident space for the purposes of planning and preparation. However, for incident response space applications of this challenge level estimation schema, there have been significant efforts in various countries to network CBRN sensors and the output of numerical weather prediction/computational fluid dynamics and atmospheric dispersion models with command and control systems, allowing automated information fusion (for source reconstruction) and response guidance [3-7] to provide improved real-time situational awareness in the CBRN battlespace, as well as to assist in rapid and dynamic decision making.

References

[1] Hoffman, W.C., Walker, T.W., Smith, V.L., Martin, D.L., and Fritz, B.K. (2007), Droplet-size characterization of hand-held atomization equipment typically used in vector control, *Journal of the American Mosquito Control Association*, **23**, 315-320.

[2] Science Applications International Corporation (1999), Hazard Prediction and Assessment Capability (HPAC), HPAC-UGUIDE-01-U-RAC0, Defense Threat Reduction Agency (DTRA).

[3] Yee, E. and Hogue, R. (2008), Advanced integrative multiscale modeling system for countering the threat of CBRN terrorism: Hazard prediction, assessment, and emergency response preparedness, NATO Modeling and Simulation Group Conference, Vancouver, British Columbia, Canada, RTO-MP-MSG-060, 39 pp.

[4] Yee, E., Lien, F.-S. and Ji, H. (2007), Technical description of urban microscale modeling system: Component 1 of CRTI project 02-0093RD, DRDC Suffield TR 2007-067, Defence R&D Canada – Suffield.

[5] Yee, E. (2010), An operational implementation of a CBRN sensor-driven modeling paradigm for stochastic event reconstruction: Technical description of an advanced modeling component of CRTI project 07-0196TD, DRDC Suffield TR 2010-070, Defence R&D Canada – Suffield.

[6] Yee, E., Lien, F.-S. and Ji, H. (2010), A building-resolved wind field library for Vancouver. Facilitating CBRN emergency response for the 2010 Winter Olympic Games, DRDC Suffield TM 2010-088, Defence R&D Canada – Suffield.

[7] Yee, E., Hoffman, I., Ungar, K., Malo, A., Ek, N. and Bourgouin, P. (2014), Bayesian inference for source term estimation: Application to the International Monitoring System radionuclide network, DRDC-RDDC-2014-R71, Defence Research and Development Canada, Suffield Research Centre.